frontiers | Frontiers in Molecular Neuroscience

TYPE Original Research
PUBLISHED 24 August 2023
DOI 10.3389/fnmol.2023.1183315



OPEN ACCESS

EDITED BY
Veronika Stoka,
Institut Jožef Stefan (IJS), Slovenia

REVIEWED BY
Hermona Soreq,
Hebrew University of Jerusalem, Israel
Vamshidhar R. Vangoor,
University Medical Center Utrecht, Netherlands

*CORRESPONDENCE
Mustafa M. Siddiq
✉ mustafa.siddiq@mssm.edu

RECEIVED 09 March 2023
ACCEPTED 04 July 2023
PUBLISHED 24 August 2023

CITATION
Siddiq MM, Toro CA, Johnson NP, Hansen J, Xiong Y, Mellado W, Tolentino RE, Johnson K, Jayaraman G, Suhail Z, Harlow L, Dai J, Beaumont KG, Sebra R, Willis DE, Cardozo CP and Iyengar R (2023) Spinal cord injury regulates circular RNA expression in axons.
*Front. Mol. Neurosci.* 16:1183315.
doi: 10.3389/fnmol.2023.1183315



# Spinal cord injury regulates circular RNA expression in axons

Mustafa M. Siddiq[1]*, Carlos A. Toro[2,3], Nicholas P. Johnson[1], Jens Hansen[1], Yuguang Xiong[1], Wilfredo Mellado[4], Rosa E. Tolentino[1], Kaitlin Johnson[2], Gomathi Jayaraman[1], Zaara Suhail[1], Lauren Harlow[2,3], Jinye Dai[1,5,6], Kristin G. Beaumont[7,8], Robert Sebra[7,8], Dianna E. Willis[4,9], Christopher P. Cardozo[2,3,10] and Ravi Iyengar[1]

[1]Pharmacological Sciences and Institute for Systems Biomedicine, Icahn School of Medicine at Mount Sinai, New York, NY, United States, [2]Spinal Cord Damage Research Center, James J. Peters VA Medical Center, Bronx, NY, United States, [3]Department of Medicine, Icahn School of Medicine at Mount Sinai, New York, NY, United States, [4]Burke Neurological Institute, White Plains, NY, United States, [5]Nash Family Department of Neuroscience, Icahn School of Medicine at Mount Sinai, New York, NY, United States, [6]Friedman Brain Institute, Icahn School of Medicine at Mount Sinai, New York, NY, United States, [7]Department of Genetics and Genomic Studies, Icahn School of Medicine at Mount Sinai, New York, NY, United States, [8]Icahn Genomics Institute, Black Family Stem Cell Institute, Icahn School of Medicine at Mount Sinai, New York, NY, United States, [9]Feil Family Brain and Mind Research Institute, Weill Cornell Medicine, New York, NY, United States, [10]Department of Rehabilitation Medicine, Icahn School of Medicine at Mount Sinai, New York, NY, United States

**Introduction:** Neurons transport mRNA and translational machinery to axons for local translation. After spinal cord injury (SCI), *de novo* translation is assumed to enable neurorepair. Knowledge of the identity of axonal mRNAs that participate in neurorepair after SCI is limited. We sought to identify and understand how axonal RNAs play a role in axonal regeneration.

**Methods:** We obtained preparations enriched in axonal mRNAs from control and SCI rats by digesting spinal cord tissue with cold-active protease (CAP). The digested samples were then centrifuged to obtain a supernatant that was used to identify mRNA expression. We identified differentially expressed genes (DEGS) after SCI and mapped them to various biological processes. We validated the DEGs by RT-qPCR and RNA-scope.

**Results:** The supernatant fraction was highly enriched for mRNA from axons. Using Gene Ontology, the second most significant pathway for all DEGs was axonogenesis. Among the DEGs was Rims2, which is predominately a circular RNA (circRNA) in the CNS. We show that Rims2 RNA within spinal cord axons is circular. We found an additional 200 putative circRNAs in the axonal-enriched fraction. Knockdown in primary rat cortical neurons of the RNA editing enzyme ADAR1, which inhibits formation of circRNAs, significantly increased axonal outgrowth and increased the expression of circRims2. Using Rims2 as a prototype we used Circular RNA Interactome to predict miRNAs that bind to circRims2 also bind to the 3'UTR of GAP-43, PTEN or CREB1, all known regulators of axonal outgrowth. Axonally-translated GAP-43 supports axonal elongation and we detect GAP-43 mRNA in the rat axons by RNAscope.

**Discussion:** By enriching for axonal RNA, we detect SCI induced DEGs, including circRNA such as Rims2. Ablation of ADAR1, the enzyme that regulates circRNA formation, promotes axonal outgrowth of cortical neurons. We developed a pathway model using Circular RNA Interactome that indicates that Rims2 through miRNAs can regulate the axonal translation GAP-43 to

regulate axonal regeneration. We conclude that axonal regulatory pathways will play a role in neurorepair.

KEYWORDS

**axons, regeneration, circular RNA, spinal cord injury, CNS, RNA-seq**

## Introduction

Axons do not spontaneously regenerate in the injured CNS. This is in part due to diminished intrinsic capability of adult CNS neurons to regenerate axons and to extrinsic inhibition at the injury site (Raineteau and Schwab, 2001; Filbin, 2003). Supraspinal neurons that synapse with spinal cord motor neurons, have cell bodies in the brain and brainstem that project axonal projections that synapse up to a meter from the cell body. These axons, have to transport multiple cargos including mRNAs from the cell body to needed areas along the axonal shaft and at the synapse (Riccio, 2018). Upon injury to the CNS, neuronal cell bodies need to transport RNAs a considerable distance away to the injury site (Willis et al., 2005, 2011; Donnelly et al., 2013; Dulin et al., 2015; Cosker et al., 2016; Spaulding and Burgess, 2017). Ribosomes are detected all along the axon and growth cone, and local translation within the axons is known to occur (Willis et al., 2005; Baleriola et al., 2014; Gracias et al., 2014; Villarin et al., 2016; Terenzio et al., 2018). The functional consequences of axonal translation are not fully known in part due to limited technologies for specifically identifying axonal mRNAs and the mechanisms by which they regulate axon growth and regeneration. Consequently, despite many studies reporting gene expression changes after spinal cord injury (SCI), there is a gap in knowledge regarding which of these expression changes occurs in descending and ascending axons responsible for voluntary movement.

The goal of this study was to define axonal mRNA profiles at the site of injury after SCI and identify the pathways modulated by differentially regulated axonal mRNAs to understand how SCI induced differentially expressed genes (DEGs) regulate axonal regeneration.

In addition to linear mRNAs, neurons express circular RNAs (Memczak et al., 2013; Rybak-Wolf et al., 2015). CircRNAs are best characterized as post-transcriptional regulators that are well conserved in mammals, particularly enriched in synapses, and expressed during differentiation (Memczak et al., 2013; Rybak-Wolf et al., 2015; Piwecka et al., 2017; Kristensen et al., 2019). Compared to their linear form, circRNAs are more stable (Kristensen et al., 2019). In the mammalian brain, circRNAs are abundant and are dynamically expressed, independent of their linear mRNA analogs (Rybak-Wolf et al., 2015). We are only beginning to understand circRNA function in maintaining brain physiology (Rybak-Wolf et al., 2015; Piwecka et al., 2017). For instance, the linear mRNA for *Rims2* encodes a presynaptic protein that is important for neurotransmitter release, but the function of circRims2 is still unknown (Wang et al., 2000; Kaeser et al., 2012). Very little is known about circRNA function and regulatory capability in neurons as a whole and if circRNA may play in axonal elongation. Elucidating the potential regulatory role of circRNAs in local axonal translation may provide a better understanding of multifaceted nature of axonal regeneration, and help in finding therapeutic targets to treat SCI.

## Methods

### SCI surgery and locomotor activity measurements

All animal experiments were performed according to ethical regulations and protocols approved by the Institutional Animal Care and Use Committee (IACUC) at Icahn School of Medicine at Mount Sinai and at the James J. Peters Department of Veterans Affairs Medical Center. Both institutes are *Association for Assessment and Accreditation of Laboratory Animal Care* (AAALAC) accredited.

Female Sprague Dawley rats 3 months of age were utilized, we utilized two animals per condition. A moderate to severe SCI at thoracic level 9 (T9) was performed using an Infinite Horizons (IH) impactor (Precision Systems and Instrumentation; Zeman et al., 2009; Toro et al., 2021). Animals were deeply anesthetized with isoflurane. A laminectomy was performed at T9. The exposed vertebral column was stabilized with clamping forceps placed rostral from T8 and caudal from T10 vertebral bodies, ensuring the exposed spinal cord is in a level horizontal plane. Control animals had laminectomy only but no contusions. The impactor tip is lowered to 3-4mms above the laminectomy site and a computer operated program is used to deliver a 250 kdyne force to the exposed spinal cord. BBB locomotor testing was done the following morning to confirm contusions were performed accurately and the animals showed no signs of spontaneous recovery [both animals were scored with a BBB of 2 (Basso et al., 1995)]. Locomotor function was evaluated in a 3-foot-wide plastic tub by two independent, blinded observers from direct observation. Animals will be recorded using a GoPro camera to provide documentation of observed behaviors.

### Tissue excision for RNA-seq

24 h after performing the SCI, we collected tissue just rostral to the injury site which contains axotomized fibers for mRNA expression profiles. Animals were deeply anesthetized and a laminectomy at T8 was performed. With sterile scissor and forceps, about 2 mm of tissue was excised just above the injury at T8. Tissue was placed into 1 ml of ice-cold Miltenyi MACS Tissue Storage Solution (Miltenyi Biotech 130-100-008). Cold active protease from *Bacillus licheniformis* (Creative Enzymes NATE0633) was added (10 mg/ml of this protease with 125 U/ml DNase in ice cold Miltenyi MACS Tissue Storage Solution; Adam et al., 2017). Cells were incubated for 7 min in a water bath set to 6°C in the cold room (Adam et al., 2017). The tissue was

triturated every 2 min for 15 s. For gentle dissociation of the tissue, a Miltenyi gentleMACS at the brain program setting was ran twice in the cold room. The sample was then incubated at 6°C for an additional 8 min with trituration. Cells are then pelleted by centrifugation at 1,200 *g* for 5 min, and supernatant was carefully collected so as not to dislodge cells. The supernatant was prepared for Bulk mRNA Sequencing. A small extract of the supernatant and cell pellet fraction were plated on glass cover slips to confirm that the supernatant was cell free and that the pellet had intact cell bodies.

## Preparation for bulk sequencing of the acellular fraction

All supernatant fraction from the spinal cord were checked for RNA integrity by Agilent 2100 Bioanalyzer and all samples had RIN value ≥9 (Stillitano et al., 2017). RNA libraries for RNA sequencing were constructed using the Truseq stranded total RNA kit (Illumina Inc.) which converts the RNA in a total RNA sample into a library of template molecules of known strand origin; and purified with a RiboZero kit (Illumina). The resulting mRNA fragment inserts were then reverse transcribed to first strand cDNA using reverse transcriptase and random primer in the presence of actinomycin D. Strand specificity was achieved during second strand cDNA synthesis by replacing dTTP with dUTP in the Second Strand marking mix which includes the DNA Polymerase I and RNase H. 3′ ends were then adenylated to prevent them from ligating to each other during the adapter ligation reaction. Unique dual index adapters (i5 and i7) were then ligated allowing for greater sample indexing diversity and enables ds cDNA for hybridization onto a flow cell. The indexed double stranded cDNA was then enriched by PCR and purified to create the final cDNA library which was quantified and then loaded on the flow cell for sequencing. 50x10E6 reads per sample were obtained for Deep analysis.

## Bulk sequencing differential expression analysis pipeline

To reduce artifacts caused by read imbalances during upper quartile normalization, we downsampled the sequencing reads of each sample to the number of reads that were detected in the sample with the lowest read counts, as described previously (Stillitano et al., 2017). Downsampled reads were aligned to the rat reference genome 'rn6' using the ensemble annotation and STAR 2.5.4b (Dobin et al., 2013) with the parameters set between outFilterScoreMinOverLread and outFilterMatchNminOverLread set to 0.33. Results of RNAseq are reported for No-SCI and SCI groups are Fragments Per Kilobase of transcript per Million mapped reads (FPKM).

According to NIH NCI GDC documentation website: https://docs.gdc.cancer.gov/Encyclopedia/pages/FPKM/#:~:text=Fragments%20Per%20Kilobase%20of%20transcript,total%20number%20of%20mapped%20reads. FPKM are a simple expression level normalization method. It is normalized based on the read counts based on gene length and the total number of mapped reads (50 million). Differentially expressed genes (DEGs) were identified with cufflinks 1.3.0 [Trapnell et al., 2010; FDR 5%, minimum $\log_2$(fold change) = +/−$\log_2$(1.3)]. Up- and downregulated genes were subjected separately and combined to pathway enrichment analysis using Wikipathways 2016 (Pico et al., 2008) and Gene Ontology biological processes 2018, downloaded from the Enrichr website (Gene Ontology Consortium, 2021), as described previously (Chen et al., 2013). From the list of over 12,000 genes detected in our screening, we manually annotated the data based on known circRNA detected in the literature to compile a list of over 200 putative circRNAs (Rybak-Wolf et al., 2015; Wu et al., 2020). The RNAseq is uploaded into GEO: GEO accession GSE230066.

## Perfusions and sectioning of spinal cord

Fresh ice-cold 4% PFA in PBS was prepared. Rats were deeply anesthetized with Ketamine and Xylazine with an $N = 4$. We transcardially perfused with ice cold PBS and then with ice cold 4%PFA in PBS. We removed the spinal cord and post-fixed them in 30% sucrose in PBS, until they sank to the bottom of the tube. Segments were embedded in OCT. Using a Leica cryostat at −20°C, we made 10 µm sections of the spinal cord to be utilized for RNAscope and immunohistological analysis.

## RNA extraction, ribonuclease R digestion, reverse transcription, and qPCR

To validate circRNA using RT-qPCR, we followed the protocol from Vromman et al. (2021) and Vromman et al. (2022), and the primer sequences we used were obtained from supplementary data on Rybak-Wolf et al. (2015). Total RNA was extracted from mouse spinal cord segments (~2 mm) rostral to the lesion epicenter 14 days after injury using TRIzol reagent (ThermoFisher) following the manufacturer's instructions and methods previously described (Zeman et al., 2009). Total RNA concentrations were determined by absorbance at 260 nm using a Nanodrop spectrophotometer (Thermo Scientific). For circRNA detection, 1,000 ng of total RNA was incubated with ribonuclease R (RNAse R; Biosearch Technologies) following the manufacturer's instructions for 20 min at 37°C followed by a cycle of 20 min at 65°C (Vromman et al., 2021). Digested RNA was later cleaned with a RNAeasy MinElute Cleanup kit (Qiagen) and reverse-transcribed into cDNA using Omniscript reverse transcriptase (Qiagen). PowerUp SYBR Green Master Mix (Thermofisher) was used to measure mRNAs of interest by qPCR. Sequence of primers used to detect both, linear and circular forms of RIMS2, VAPA and RTN4 were as previously reported (Rybak-Wolf et al., 2015) for: linear RimS2 Fw: GCAAAACTACACGAGCAGCC and Rv: TCCCT GGACACTGATGGACT; circular RimS2 Fw: AAAGTCGCAGT GCCTCTCAA and Rv: TCCCATCCTGAGCGATACTTC; linear Rtn4 Fw: CAGTCCTGCCCTCCAAGC and Rv: TCAGATGC AGCAGGAAGAGC; circular Rnt4 Fw: AGATCCCTGAC AGCTGTATTGT and Rv: GACGAAACAGTGTTACCTGGC; linear Vapa Fw: TGTTTGAAATGCCGAATGAA and Rv: AGTCGCTT GCACTCTTCCAT; circular Vapa Fw: TGTTTGAAATGCC GAATGAA and Rv: AGTCCTTGCACTCTTCCAT. Formation of single SYBR Green-labeled PCR amplicons were verified by running melting curve analysis. Threshold cycles (CTs) for each PCR reaction were identified by using the QuantStudio 12 K Flex software. To construct standard curves, serial dilutions were used from 1/2 to 1/512

of a pool of cDNAs generated by mixing equal amounts of cDNA from each sample. The CTs from each sample were compared to the relative standard curve to estimate the mRNA content per sample; the values obtained were then normalized using peptidylprolyl isomerase A (Ppia) mRNA.

## RNAscope

We utilized RNAscope Multiplex Fluorescent v2 Assays (ACD biosciences). We followed the manufacturers protocol with minor modifications (Kang et al., 2023). Spinal Cord sections were post-fixed with 4%PFA, washed in PBS. Followed by ethanol series dehydration and subsequent rehydration series prior to treatment with hydrogen peroxide and washed again with water 3 times. Antigen retrieval was done by protease III (for cortical neurons in culture) or protease IV (for spinal cord sections) treatment in PBS for 10 min at RT; slides will then be washed twice with PBS. Sections were hybridized with probes for 2 h at 40°C then washed with wash buffer. Hybridized probes were detected using the RNA-scope Amplification (Raineteau and Schwab, 2001; Filbin, 2003; Riccio, 2018) reagents for 30 min at 40 C. Slides were washed and then incubated with Opal dyes (Akoya biosciences) for 15 min at 40 C. Immunohistochemistry were by performed as follows. Sections were permeabilized with 0.25% Triton-X then blocked with 10% goat serum in TBS with 1%BSA overnight at 4°C. Some sections were be co-labeled with antibody for β-III tubulin in TBS-BSA overnight, washed and incubated with secondary goat-anti mouse coupled to Alexa-405 for 1 h at RT. Slides were washed and coverslips mounted with ProLong Gold antifade.

For Ribonuclease R digestion, after the Protease step and 3 washes with PBS, we permeabilized the tissue with 0.1% Tween-20 in PBS for 10 min at RT. Then washed the samples with PBS three times. All RNAscope experiments were performed a minimum of 3–4 independent times.

## Rat and mouse primary cortical neuronal cultures

Rat and mouse primary cortical neuronal cultures were prepared as previously described with minor modifications (Siddiq et al., 2015, 2021) were dissected from postnatal day 1 Sprague Dawley rat brains and C57BL6 mouse brains, from both sexes. Mouse cultures were utilized for RT-qPCR analysis with siRNA ablation for ADAR, since the unique junctions sites and primers specific for circRNA are better described for mice than for rats. The cortices were incubated twice for 30 min with 0.5 mg/ml papain (Sigma) in plain Neurobasal (NB) media (Invitrogen) supplemented with DNase. At the end of the second digestion with papain, the cortices were pipetted through a 1 ml serological pipette in a low volume (2 to 3 mls), to dissociate the tissue. The triturated tissue for every 3 cortices was made up to 6mls with plain NB and strained through a 70micron cell strainer. The cell suspensions were layered on an Optiprep density gradient (Sigma) and centrifuged at 1,900x*g* for 15 min at room temperature, with the brakes decreased to the lowest setting to not disrupt the gradients. The layer closest to the bottom between 1 to 2mls of a 15 ml conical tube is the enriched fraction of neurons. The enriched neuronal layer was then pelleted at 1000 x g for 5 min and counted.

## Microfluidic neurite outgrowth assay

Square microfluidic chambers (SND450, 450 µm microgroove) were purchased from Xona microfluidics. The chambers were sterilized under UV for 15 min and soaked in 70% ethanol for 2 min and allowed to air dry under a sterile TC hood. We used MatTek dishes (P50G-1.5, MatTek corp.) that we pre-coated with PLL overnight and then rinse 3 times with sterile water and air dried overnight in a TC BSL2 hood. Using autoclaved forceps we carefully place the microfluidic chamber on the glass area of the MatTek dish, and gently apply pressure to ensure the chambers are sitting on the glass. Primary cortical neurons were diluted to 5x10E6 cells/ml in NB supplemented with B27, L-glutamine and antibiotics, and in a final volume of 200µls. Approximately 15µls of the cell suspension was carefully inserted into the top well of one side of microfluidic chamber. We then placed the Mat-tek dishes with the microfluidic chambers inside a 37°C incubator for 20 min to allow the neurons to adhere. All wells were filled with 150µls of supplemented NB. Once we observe neurites growing across the microgroove (3-4 days), we then performed an axotomy.

To quantify the outgrowth we immunostained using a monoclonal antiβIII tubulin antibody (Tuj1;Covance) and Alexa Fluor −405- (Blue) or 488- (Green) conjugated anti-mouse IgG (Invitrogen). For quantification, images were taken, and the length of the longest neurite for each neuron was measured using MetaMorph software (Molecular Devices). All imaging was performed on a Zeiss LSM 880 confocal microscope.

## siRNA transfection

All siRNA were purchased from Accell smartpool siRNA (Thermo Scientific), following the manufacturers protocol. We targeted ADAR1 for rats (Rat Accession number XM_006232778.3) and mice (Mouse Accession number NC_000069.7), scrambled non-targeting siRNA was also utilized for controls. Cortical neurons were plated on one side of the microfluidic chambers. We waited 2–4 h after plating to allow the cells to adhere. Utilizing 1 µM siRNA in 150µls of Accell Delivery Media was added to the neuronal cell bodies and incubated overnight at 37°C incubator. All siRNA experiments were performed a minimum of 3–4 independent times. The next morning, we added 150µls of supplemented NB. We incubated for a further 72 h before stopping the experiment with 4% paraformaldehyde and 4% sucrose. We then stained the chambers with β-III tubulin (Alexa-488) and in individual neurons panel, we also used Actin-Red staining (Thermo Scientific) and quantified the neurite length. For RT-qPCR, at the 72 h timepoint the wells were washed with ice cold PBS and lysed with 1 ml Trizol and immediately flash frozen in liquid nitrogen.

## Statistical analyses

All analyses were performed using GraphPad Prism software, and data are represented as mean ± SEM. Statistical significance was assessed using paired one-tailed Student's *t* tests to compare two groups, and one-way ANOVAs with Bonferroni's *post hoc* tests to compare between three or more groups.

# Results

## mRNAS and circular RNAS in axons

We adapted a tissue dissociation protocol used for single cell RNAseq (scRNAseq) that uses cold active proteases to gently dissociate tissue and isolate cells (Adam et al., 2017). Low speed centrifugation of the dissociated cell suspension was used to pellet cells and recover the supernatant. This was followed by bulk RNA sequencing (RNAseq) of the supernatant to identify mRNAs associated with the acellular fraction of cells. We identified the DEGS by comparison of RNAseq data for control vs. SCI groups and then assigned the DEGS to different cell types based on published single-cell transcriptomic studies (Zeman et al., 2009; Hansen et al., 2019; van Hasselt et al., 2020). The DEGS are shown in Table 1. We detected 3 known axonal microtubule associated protein (MAP) mRNAs, MAP4, Tau (MAPT) and MAP7 and all were significantly down-regulated after SCI. MAP4 was the most abundant axonal mRNA detected. Several axonal RNA transport mRNAs were detected. RBP1 is up-regulated nearly 15-fold after SCI (Kar et al., 2018; Sleigh et al., 2019). We detected RNAs that function in the molecular motors that drive anterograde transport (Kinesins such as KIF5A), and retrograde transport (Dynein, DYNC1LI2; Balabanian et al., 2018). Other mRNAs detected included those encoding Guanine Deaminase (GDA), MACROH2A1, IMPACT and Rims2.

In Table 2, we show detection of the dendritic marker MAP2, but its levels are over 10-fold lower than the axonal MAP4 detected in Table 1. We did not detect the following astrocytic markers: Glial fibrillary acidic protein (GFAP), S100B, Excitatory amino acid transporter 1 and 2 (EAAT1 and 2) and aquaporin 4 (AQP4), but did observe low level expression of ALDH1L1 (Nagelhus and Ottersen, 2013; Escartin et al., 2021; Sun et al., 2022). Microglial markers, such

TABLE 1 DEG analysis indicates enrichment for axonal RNA.

| DEG | No-SCI | SCI | P-Adj | Log2 Fold |
|---|---|---|---|---|
| Axonal Markers | | | | |
| Axonal MAPs | | | | |
| MAP4 | 20198.17 | 6958.2 | ***0.014066*** | −1.537438 |
| MAPT (tau) | 2,223 | 1231.45 | ***0.013229*** | −0.8521476 |
| MAP7 | 712.95 | 220.02 | ***3.92E-13*** | −1.695605 |
| Axonal mRNA Transport | | | | |
| RBP1 | 92.79 | 1467.37 | ***1.81E-12*** | 3.983084 |
| Axonal Anterograde | | | | |
| KIF5A | 36.6375 | 15.52 | ***1.79E-02*** | −1.239592 |
| Axonal Retrograde | | | | |
| DYNC1LI2 | 1595.324 | 570.756 | ***6.66E-08*** | −1.482903 |
| **DEGs** | | | | |
| GDA | 6.74 | 51.19 | ***1.07E-06*** | 2.926016 |
| NGF | 2.77 | 12.18 | ***0.001586*** | 2.137659 |
| MACROH2A1 | 243.62 | 607.32 | ***0.026033*** | 1.31786 |
| NCAM1 | 202.47 | 82.65 | ***2.51E-06*** | −1.292713 |
| IMPACT | 22.42 | 8.6 | ***0.0298*** | −1.382178 |
| Rims2 | 183.564 | 68.53 | ***0.00026*** | −1.421475 |

Axonal markers DEGS detected when comparing uninjured rat spinal cord (No-SCI) to ones that received contusions to the spinal cord (SCI). The values shown for No-SCI and SCI are Fragments Per Kilobase of transcript per Million mapped reads (FPKM). According to NIH NCI GDC documentation website: (https://docs.gdc.cancer.gov/Encyclopedia/pages/FPKM/#:~:text=Fragments%20Per%20Kilobase%20of%20transcript,total%20number%20of%20mapped%20reads). FPKM are a simple expression level normalization method. It is normalized based on the read counts (we do 50 million reads) based on gene length and the total number of mapped reads. P-Adj (Q-) values adjusted for multiple comparison testing and Fold changes are shown. Significant Q-values are in Bold and Italic type. Fold changes are presented as Log2 fold changes. We made a short list of both novel and known DEGs (green font). For our Bulk RNA-seq analysis we read 50×10E6 reads per sample, giving us the ability to detect low abundance transcripts. Bold and italic numbers for P-Adj indicate significant change.

TABLE 2 DEG analysis suggests minimal glial cell contamination.

| DEG | No-SCI | SCI | P-Adj | Log2 Fold |
|---|---|---|---|---|
| Dendritic markers | | | | |
| MAP2 | 2139.92 | 859.51 | ***0.000225*** | −1.315974 |
| Astrocytic markers | | | | |
| GFAP | Not Detected | | | |
| S100B | Not Detected | | | |
| EAAT1/GLT1 | Not Detected | | | |
| EAAT2 | Not Detected | | | |
| AQP4 | Not Detected | | | |
| ALDH1L1 | 8.19166 | 3.01872 | ***3.32E-05*** | −1.44022 |
| ALDOC | Not Detected | | | |
| SLC1A3 | Not Detected | | | |
| Microglia markers | | | | |
| Iba1 | Not Detected | | | |
| P2YR12 | Not Detected | | | |
| TMEM119 | 8.66 | 6.49 | 0.659135 | −0.4151374 |
| SPP1 | 221.958 | 265.43 | 0.703813 | 0.2580448 |
| TREM2 | 21.771 | 32.834 | 0.516 | 0.5927786 |
| AXL | 39.485 | 22.511 | 0.276637 | −0.8107108 |
| LPL | 3.096 | 1.752 | 0.07306 | −0.8213534 |
| CST7 | 3.682 | 6.166 | 0.478 | 0.7437049 |
| Oligodendrocyte | Markers | Associated | with cell bodies | |
| MBP | Not Detected | | | |
| APC | 185.118 | 111.813 | 0.052068 | −0.727355 |
| NG2 | Not Detected | | | |
| O4 | Not Detected | | | |
| MOG | 138.127 | 63.8503 | 0.137524 | −1.11323 |
| Oligodendrocyte | Markers | Associated | with cell | processes |
| CNP | 1887.484 | 614.932 | ***0.016289*** | −1.61797 |
| RIP | Not Detected | | | |
| GALC | 10.114 | 6.4 | 0.528041 | −0.66017 |
| OMGP | Not Detected | | | |
| MAG | 271.936 | 87.3568 | ***9.69E-06*** | −1.63828 |

The table lists DEGs of known dendritic and glial cell markers. Adjusted *p* values, corrected for multiple comparison testing and fold changes are shown. Bold numbers indicate significant change.

as Iba1 and P2YR12, were not detected. Several microglial cell markers were detected at low levels, but there was no difference in their P-Adj value when comparing controls and SCI (Gong et al., 2013; Raj et al., 2017; Sugiyama et al., 2019; Wang et al., 2020; Cao et al., 2021; Schwabenland et al., 2021; Sun et al., 2022). In general, the number of transcripts associated with microglial markers was relatively low (<100), whereas there were >10,000 axonal-associated markers detected. We have mixed results for detection of oligodendrocyte markers, but only CNP and MAG were significantly altered by SCI (CNP) which are known markers for the oligodendrocyte processes that myelinate axons, suggesting that we are detecting processes associated with the axons and not the oligodendrocyte cell bodies (Bradl and Lassmann, 2010; Miron et al., 2011). Taken together, the robust axonal signals that are associated with axonal markers with minimal dendritic and glial cell contamination, indicate that we had enriched the supernatant fraction for axonal RNA (Figure 1).

We also looked for known markers of Spinal Interneurons (Table 3 and in Supplementary Table 1). Only a few (ASCL1, CBLN2, GAD2, RORA, RORB, and SMARCA2) of the interneuron sub-type specific marker RNAs were detected. These had low abundance and were not significantly altered by SCI. We also looked for motor neuron markers and found that roughly half of them were undetected. For the remaining mRNA species for motor neurons, 5 were significantly altered by SCI and 4 of the motor neuronal markers (RUNX1, ZEB2, FOXP1, and FOXP2) have also been reported to be either in the axons or involved in mediating axonal elongation (König et al., 2011; Vernes et al., 2011; Adams et al., 2015; Hegarty et al., 2017). Overall, our analysis indicates that we do have enrichment of axonal RNA (see Tables 1–4; Supplementary Table 1) with minimal contaminating glial cells, spinal interneurons, or motor neurons (Figure 2). By Gene Ontology analysis, the second most significant pathway for all DEGs was axonogenesis, as well as other specific neuronal processes such as synaptic transmission and neurogenesis (Figure 2).

We validated the expression of selected DEGs in axons of cultured primary rat cortical neurons plated in microfluidic chambers using RNA-scope. RNAscope enables us to visualize single RNA

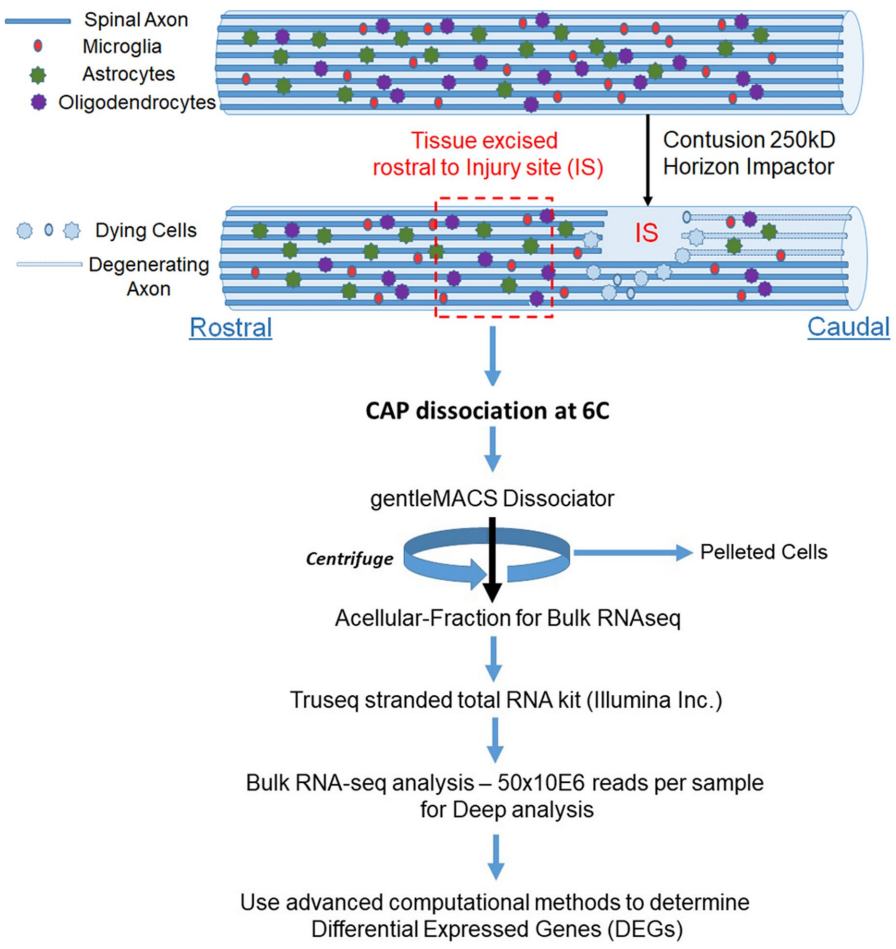


FIGURE 1
Schematic for enrichment of acellular RNA from the spinal cord. Adult Sprague Dawley rats have laminectomies at T9 and performed contusions using an Infinite Horizons impactor with a force of 250kdyne to induce SCI, while control animals have laminectomy only. We utilized two animals per condition. We wait 24 h and then excised tissue approximately one lamina rostral from the injury site (IS) and treated with CAP at 6°C. We used the gentleMACS Dissociator in the cold room set to the Brain setting and then centrifuged the sample at 1200RPM for 5 min. We used the supernatant fraction for Bulk RNA-seq. We identified DEGs between laminectomy alone vs. SCI. We used Gene ontology to identify biological processes (pathways) from DEGs.

TABLE 3 DEG analysis suggests minimal spinal interneuron RNA.

| DEG | No-SCI | SCI | P-Adj | Log2 Fold |
|---|---|---|---|---|
| Interneurons | | | | |
| ASCL1 | 2.01347 | 2.88741 | 0.51936 | 0.520092 |
| BARH1 | Not Detected | | | |
| BRN3A | Not Detected | | | |
| BRN3B | Not Detected | | | |
| CBLN2 | 6.23645 | 2.839465 | 0.162549 | −1.135106 |
| DRG11 | Not Detected | | | |
| GAD2 | 2.78046 | 1.833779 | 0.183802 | −0.6005038 |
| GLYT2 | Not Detected | | | |
| GSH1 | Not Detected | | | |
| GSH2 | Not Detected | | | |
| ISL1 | Not Detected | | | |
| LHX1 | Not Detected | | | |
| LHX2 | Not Detected | | | |
| LHX5 | Not Detected | | | |
| LHX9 | Not Detected | | | |
| LMX1B | Not Detected | | | |
| MATH1 | Not Detected | | | |
| NPY | 302.955 | 221.5497 | 0.700791 | −0.4514731 |
| PAX2 | Not Detected | | | |
| PTF1A | Not Detected | | | |
| RORA | 52.0532 | 35.422 | 0.526817 | −0.5553411 |
| RORB | 9.1919 | 6.02137 | 0.4115 | −0.6102714 |
| SMARCA2 | 7.78941 | 7.35343 | 0.927974 | −0.08309677 |
| TAG-1 | Not Detected | | | |
| TLX-3 | Not Detected | | | |
| VGLUT2 | Not Detected | | | |

DEGs of spinal interneuron markers. Adjusted *p* values and fold change are shown. Additional markers can be found in Supplementary Table 1.

TABLE 4 DEG analysis for Motor Neuron RNA.

| DEG | No-SCI | SCI | Q-value | Fold Change |
|---|---|---|---|---|
| Motor Neurons | | | | |
| HB9 | Not Detected | | | |
| ISL1 | Not Detected | | | |
| ISL2 | Not Detected | | | |
| LHX3 | Not Detected | | | |
| FOXP1 | 25.43917 | 147.0716 | ***0.00034924*** | 2.531395 |
| FOXP2 | 1.146702 | 4.91447 | ***3.25E-07*** | 4.285743 |
| ALDH1A2 | 4.39558 | 61.0843 | ***1.87E-12*** | 13.89675 |
| ALCAM | 11.6908 | 10.45785 | 0.883312 | 0.8945367 |
| RUNX1 | 14.94835 | 43.8459 | ***0.021013*** | 2.93316 |
| PHOX2B | Not Detected | | | |
| POU3F1 | Not Detected | | | |
| SMAD1 | 53.63974 | 57.01732 | 0.940752 | 1.062968 |
| NOS1 | Not Detected | | | |
| ZEB2 | 151.9246 | 80.1586 | ***0.0122304*** | 0.5276209 |
| ETV1 | 588.7746 | 384.8541 | 0.304098 | 0.6526527 |

The table lists motor neuronal marker DEGs. Adjusted *p*-value and fold change are given. Bold numbers indicate significant changes Supplementary Table 1.

molecules within a cell using confocal laser microscopy. One novel DEG detected was GDA which can promote microtubule assembly in neurons, a necessary step for axonal extension, which is up-regulated after SCI (Akum et al., 2004). In Figure 3, we show validation of the RNAseq detected DEGs using RNAscope. We also probed for GAP-43, which was known to be located in the axons (Donnelly et al., 2013). We observed that GAP-43 (green) and GDA (red) were present in the cell bodies (Figure 3A left side and Figure 3H). 24 h post axotomy, the expression of both GAP-43 and GDA (Figure 3H) was increased compared to no axotomy control. Elevated GAP-43 expression was anticipated, as it is known to be elevated in neurons after CNS injury (Doster et al., 1991; Curtis et al., 1993). In addition to the increased axonal mRNA levels, both GAP-43 and GDA mRNAs are transported to more distal axonal regions following axotomy (see magnified region in Figure 3D, quantification in Figures 3F,G). The graphs in Figures 3G,H are the average of 4 independent experiments for which RNA was quantified blindly by two independent reviewers. We also examined other DEGs, such as NGF and IMPACT. NGF has a well established role in growth support of neurons and promoting neurite outgrowth and axonal extension (Mocchetti and Wrathall, 1995). IMPACT is found in the CNS, having a role as a translational regulator (Waller et al., 2012). In Figure 3E we show an axon exiting the microgroove and both NGF (red) and IMPACT (green) were detected but they were localized to different regions of the axons. We further validated additional DEGs detected in both cortical neurons and in adult rat spinal cord. We detected MACROH2A1 (red) and MAP4 (green) in cortical neurons in microfluidic chambers and in sectioned uninjured rat spinal cord by RNAscope (Figures 4A,B) and found their movement increases after axotomy. A second sample with a magnified region a axotomized sample displays the robust labeling of the axons with MAP4 and distribution of MACROH2A1 along the axons immunostained with β-III tubulin (blue; Figure 4B). MACROH2A1 is a variant of histone H2A; its depletion in mouse brains has been shown to boost hippocampal synaptic plasticity (Chiodi et al., 2021). Quantification of average distribution and distance from the microgroove edge are shown to the right of images ($N = 4$). With axotomy, more MAP4 and MACROH2A1 RNA are detected further along the axon when comparing to no axotomy control.

We examined localization of selected DEGs in rat spinal cord sections using RNAscope. The RNA for MACROH2A1 (red) and MAP4 (green) by RNAscope (Figure 5A), localized in the white matter outside of the DAPI (blue) stained nuclei. In a sagittal section of the rat spinal cord, we immunostained for β-III tubulin (blue) and detected the mRNA for MACROH2A1 (red) by RNAscope (Figure 5B), that co-localized with the β-III tubulin. Since we are interested in axonal translation, we also confirmed the expression of S6 Ribosomal Protein in the growing axons by immunohistochemistry (Supplementary Figure 3). Ribosomes were detected in the growth cone tip detected by Actin (red, see arrow) and along the axonal shaft with β-III Tubulin.

One DEG decreased after SCI was Rims2. Rims2 is reported to be predominately a circular RNA (circRNA) in the rodent brain

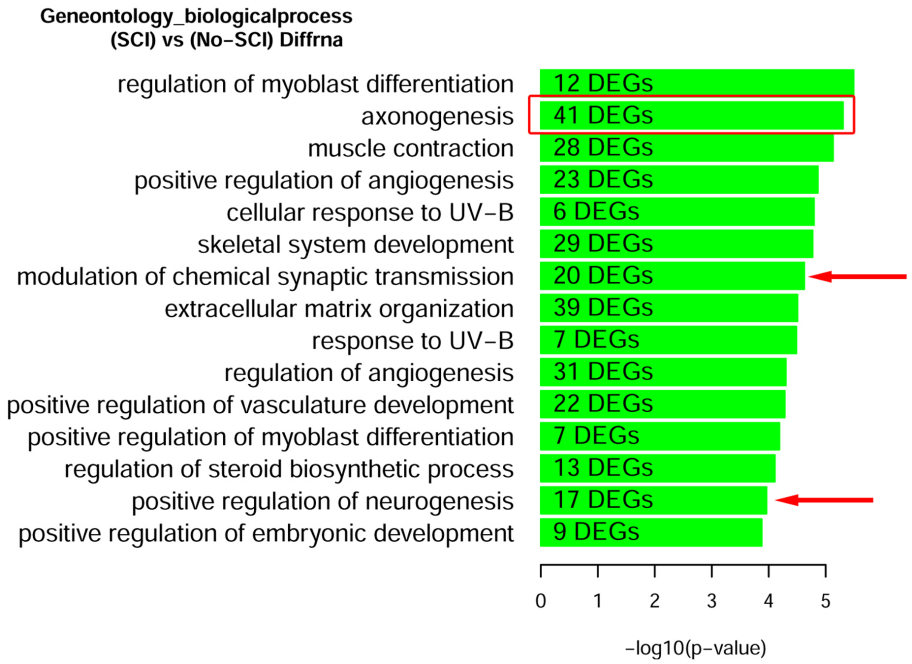


FIGURE 2
Gene Ontology enrichment of DEGs after SCI identifies that axonogenesis is a robustly significant biological processes. Rats with and without spinal cord injury (SCI) were subjected to CAP purification for the acellular fraction for Bulk RNA-seq analysis. Lists of DEGs were used for enrichment analysis to predict differentially regulated pathways. We find the second most significant pathway to be for Axonogenesis (red box). Other pathways relevant to the CNS are demarcated with a red arrow. A complete list of Up-regulated and Down-regulated GO-pathways is shown in Supplementary Figure 1.

(Rybak-Wolf et al., 2015). We therefore manually annotated over 12,000 genes detected in our RNA-seq for known circRNAs by searching the literature and using the known literature for identified circRNAs, in particular Rybalk-Wolk A, Mol Cell. 2015 Jun 4;58 (Dulin et al., 2015):870–85. doi:10.1016/j.molcel.2015.03.027 and circAtlas - https://ngdc.cncb.ac.cn/circatlas/, amongst others (Memczak et al., 2013; Rybak-Wolf et al., 2015; Piwecka et al., 2017; Kristensen et al., 2019; Vromman et al., 2021, 2022). We found over 200 putative circRNAs in our RNAseq data. In Tables 5A,B we list the top 20 most significantly altered putative circRNAs found. Down-regulated circRNAs are in Table 5 and the up-regulated ones are in Table 5B. We confirmed by RT-qPCR in combination with digestion by ribonuclease R (RbnR, an enzyme that can only digest linear mRNAs but not digest circRNAs), that we could detect the circRNAs for Rims2, RTN4 and VAPA in mouse spinal cord tissue with and without contusion (Figure 6). Supporting the RNA-seq analysis, RT-qPCR for both Rims2 and RTN4 confirmed that their mRNAs were significantly downregulated after SCI, while VAPA was up-regulated.

## Role of circRNA in axonal regeneration

To determine if circRNAs are involved in axonal regeneration, we knocked down the RNA editing enzyme ADAR1 by siRNA in primary rat cortical neurons (Ivanov et al., 2015). ADAR1 antagonistically regulates the formation of circRNAs (Ivanov et al., 2015). Ablation of ADAR1 should lead to an increase in circRNA levels. We first checked if ADAR 1 ablation affects the neurons at a functional level. ADAR1 ablation led to increases in axonal outgrowth (Figure 7). We confirmed by RT-qPCR that ADAR1 siRNA was decreasing ADAR1 expression by over 60% reduction (Supplementary Figure 2A). Controls (with scrambled siRNA) grew axons up to a maximum of 900 µm from the edge of the microgrooves ($N = 4$). ADAR1 knockdown resulted in longer (1.2 mm from the microgroove) and more abundant outgrowth (Figures 7B,C) at 800 and 900 µm from the edge of the microgrooves. RT-qPCR of cortical neurons with ADAR1 siRNA knockdown demonstrated significantly higher levels of the axonal specific marker, MAP4 (Figure 7D). We also determined that ADAR1 siRNA treatment significantly increases circRimS2 levels compared to scrambled controls (white) and promotes neurite outgrowth (grey; Figure 7E). There is also a trend for circRTN4 being elevated with ADAR1 siRNA (grey; $N = 4$, $p$-value 0.0532) compared to scrambled controls (white).

We confirmed the presence of circRims2 in rat spinal cord (Figure 8). Adjacent sections of uninjured spinal cord from the same animal were used for RNAscope detection of GAP-43 (green) and Rims2 (red) transcripts with β-III tubulin (blue) immunohistochemistry. One section was treated with ribonuclease R (right image) to eliminate linear transcripts (GAP-43) and linear Rims2; the adjacent section was used as an untreated control. Both transcripts were present in untreated sections; with ribonuclease R treatment, GAP-43 expression was absent, but Rims2 was detected indicating that it is circular and therefore protected from the ribonuclease.

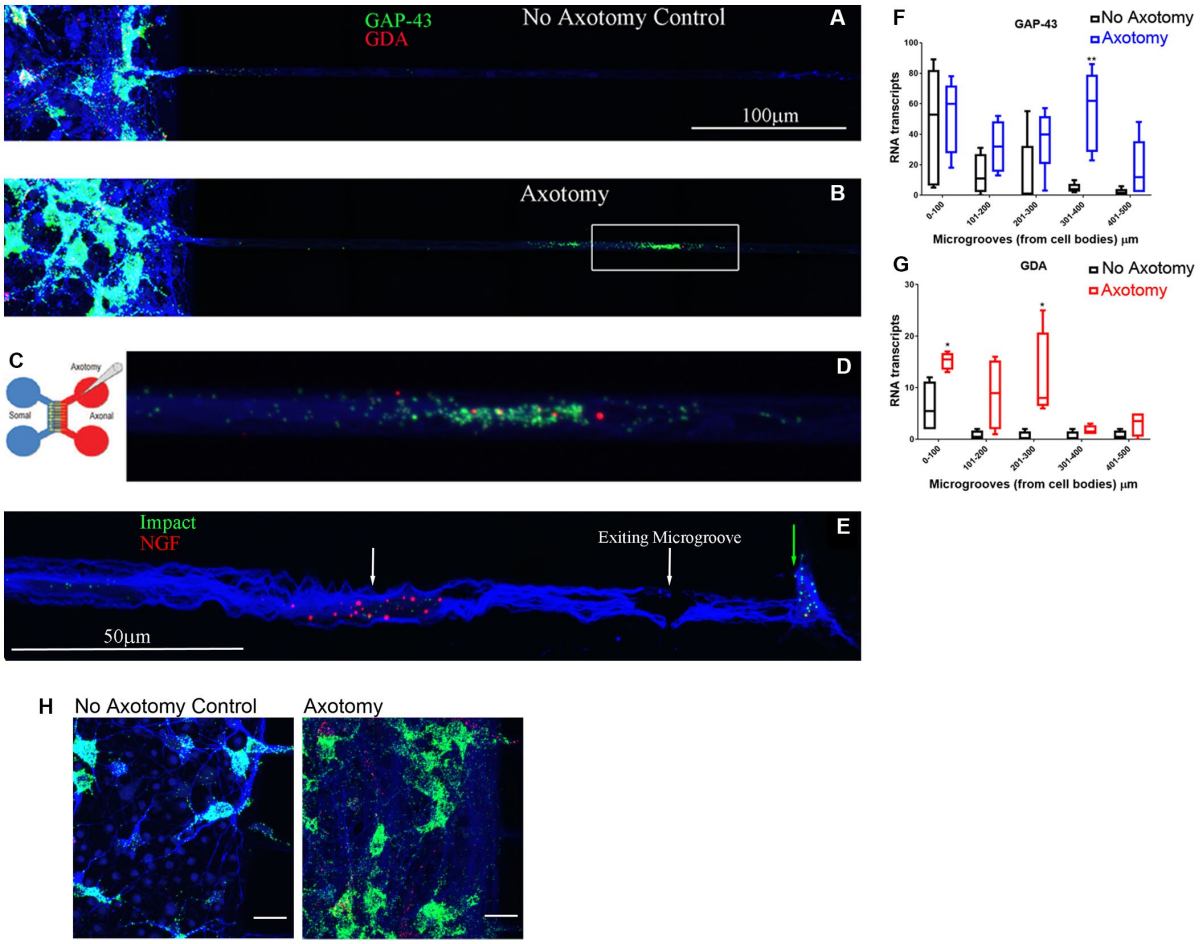


FIGURE 3
DEGs found from the RNA-seq data detected in growing axons using RNAscope. Primary rat cortical neurons were plated in microfluidic chambers and given 4days to put axons across the microgrooves and into the axonal chamber. On day 4 we performed an axotomy and waited 24h (see Cartoon of microfluidic chambers in **C**), where we sever the growing axons from the somal compartment. Comparing no axotomy controls **(A)** to lesioned axons **(B)** we see that in the cell body side (somal) on the left, there is in increase in GAP-43 (green) in the neuronal cell bodies that had axotomy in **(B)**. We also observed in the microgrooves of the lesioned axons, there was more abundant GAP-43 and GDA (red) in the microgrooves. The white box in **(B)** is shown in higher magnification in **(D)**, displaying the GAP-43 and GDA RNA. The axons are observed by immunohistochemical staining for β-III tubulin which is shown in blue. **(E)** Using RNAscope for Impact (Green) and NGF (Red), and looking in the microgrooves as the axons are exiting from them, we see a spatial distribution of NGF in the axons (see white arrow) comparing to Impact (see green arrow) which is found at the growing tip of the axons. We preformed 4 independent experiments for each condition. **(F)** Quantification of GAP-43 RNA in 100 micron increments within the microgroove with and without axotomy. The graph is the average of 4 independent experiments. **(G)** Quantification of GDA RNA in 100 micron increments within the microgroove with and without axotomy. The statistics is t-test with $*p < 0.05$ and $**p < 0.01$. **(H)** Closeup image of the cell bodies with and without axotomy and probed by RNAscope for GAP-43 (green) and GDA (red).are shown As predicted from MRNA-Seq data both GAP-43 and GDA should be elevated after axotomy and this is what we observe. The neurons are also immunostained with β-III tubulin which is shown in blue.

## A potential RNA regulatory pathway in axons

Since the known roles for circRNA are to serve as miRNA 'sponges' or to bind to RNA-binding proteins (RBP; Memczak et al., 2013; Piwecka et al., 2017; Kristensen et al., 2019), we took a bioinformatics approach by using Circular RNA Interactome to determine which miRNA or RBP could be binding to circRims2 (Dudekula et al., 2016). We detected several miRNAs that have been implicated in regulating axonal outgrowth, such as miR-155 (Gaudet et al., 2016, 2018), miR-21 (Kar et al., 2021) and miR-377 and -192. The latter two miRNAs also target GAP-43 (Liu et al., 2020; Li et al., 2021). From this bioinformatics analyses, we hypothesize an RNA pathway in axons from circRims2 to GAP-43 mRNA. Such a pathway would be able to regulate the local levels of GAP-43 protein (Dudekula et al., 2016). Additionally, we find that circRims2 can interact with the RBP, FUS, which is involved in neurite outgrowth (Supplementary Figure 4; Orozco et al., 2012; Guo et al., 2017; Ishigaki and Sobue, 2018; Birsa et al., 2021).

# Discussion

Identifying the axonal RNAs transported to the site of axotomy in the injured spinal cord is critical to determining which of these

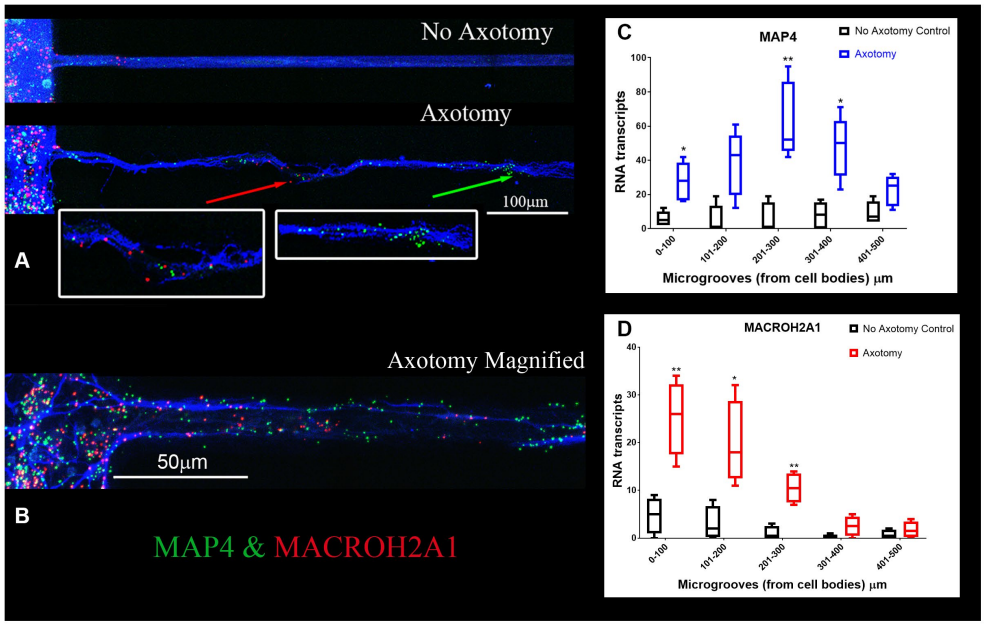


FIGURE 4
MACROH2A1 and MAP4 RNA are detected in axons with axotomy. **(A)** Cortical neurons in microfluidic chambers without axotomy have little detectable MACROH2A1 (Red) and MAP4 (Green) by RNAscope in growing axons immunostained with β-III tubulin (Blue). After Axotomy both multiple transcripts of MACROH2A1 (red arrow) and MAP4 (green arrow), several hundred microns further away when comparing to No Axotomy. We preformed 4 independent experiments. **(C)** Quantification of MAP4 RNA in 100 micron increments within the microgroove with and without axotomy. The graph is the average of 4 independent experiments. **(D)** Quantification of MACROH2A1 RNA in 100 micron increments within the microgroove with and without axotomy. The statistics is t-test with $*p < 0.05$ and $**p < 0.01$. The neurons are also immunostained with β-III tubulin which is shown in blue.

may be required for promoting axonal repair. A reliable technique for determining specific axonal RNA without contaminating glial cell or spinal neuronal cell bodies RNA has been lacking. Here, we report a simple procedure for enriching axonal fractions of spinal cord incorporating cold active proteases that function at 6°C that helps reduce artifacts from transcription or translation of RNA that can occur with enzymatic digestion at 37°C (Figure 1; Adam et al., 2017). Our analysis indicates the enrichment of axonal RNA (see Tables 1–4; Supplementary Table1). Intriguingly, the only significant DEG for oligodendrocytes detected were for CNP and MAG, which are known to be associated with myelinating processes that ensheath axons (Bradl and Lassmann, 2010; Miron et al., 2011). Though no significant spinal interneurons markers were detected, we detected five motor neuron (MN) marker RNAs that were significantly modulated when comparing control preparations to SCI. In the literature, 4 of these 5 mRNAs (RUNX1, ZEB2, FOXP1 and FOXP2) have also either been detected in the axons or are involved in axonal outgrowth (Bradl and Lassmann, 2010; König et al., 2011; Miron et al., 2011; Hegarty et al., 2017) and hence we cannot rule out that they are axonal in origin. We validated that the DEGs detected by RNAseq could be detected in the growing axons of cortical neurons in culture and in the white matter of the adult rat spinal cord. Similar to what has been reported for GAP-43 elevation after axon injury, we observed elevated GAP-43 levels after axotomy of cortical neurons (Figure 3H; Doster et al., 1991; Curtis et al., 1993). In our RNA-seq dataset, we detected a novel DEG, GDA, which is found at synapses, and which increases significantly after injury (Akum et al., 2004). We confirmed by RNA-scope that not only do GDA levels go up after axotomy but GDA transcripts travel significantly further down the axons growing in the microgrooves (Figure 3). Similarly, MACROH2A1, which is elevated after SCI, and we detect it in the axons of cortical neurons (Figure 4) as well as in the white matter of the spinal cord outside of the neuronal cell bodies (Figure 5). These findings support the conclusion that we are indeed detecting axonal localized RNAs.

An important consideration was the detection of MAP4 in our primary neuronal cultures isolated from pup brains compared to adult spinal cord (see Figures 4, 5). Though MAP4 was detected in both primary neurons and in the spinal cord, MAP4 RNA was expressed in higher levels and moving along the growing axons that had been severed in our microfluidics chambers. MAP4 protein is associated with microtubules and after axotomy axons were regrowing with an observed increase in MAP4 mRNA. While adult animals with spinal cord which do not spontaneously recover after SCI, we observed a decrease in MAP4 levels from our RNA-seq. These differences in MAP4 expression could be attributed to young neurons growing on a permissive substrate to regrow axons (hence increasing MAP4) compared to adult animals that have far less spontaneous regrowth and diminished detection of MAP4.

One DEG in the axon, Rims2, has been found to be predominately a circRNA in the rodent brain (Rybak-Wolf et al., 2015). We detected circRims2 by RT-qPCR in combination with ribonuclease R treatment in spinal cord tissue. Similar to what we observed from our RNA-seq analysis, we observed that Rims2 goes down significantly after injury

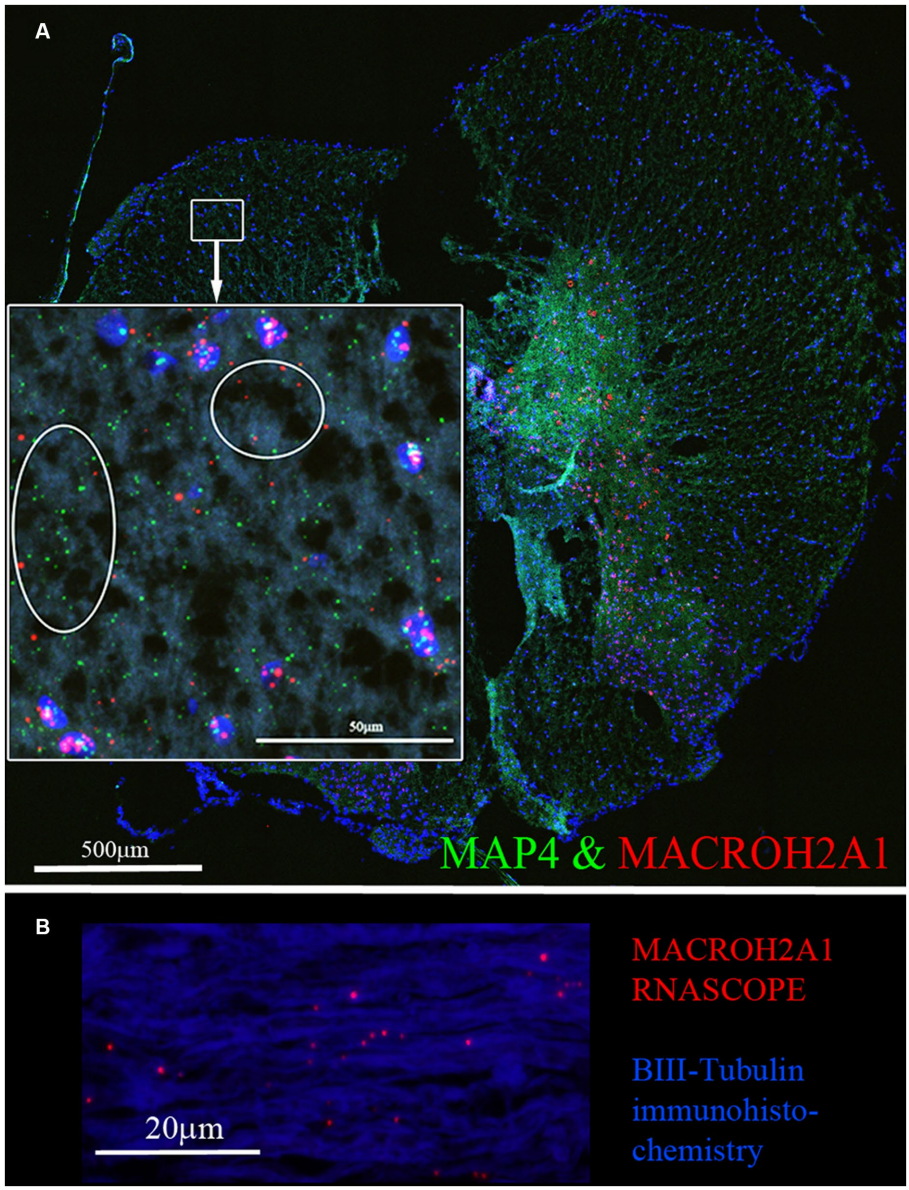


FIGURE 5
**(A)** MACROH2A1 and MAP4 RNA are detected in the white matter of rat spinal cord. Both MACROH2A1 and MAP4 transcripts are detected by RNAscope in the white matter of the uninjured rat spinal cord in the transverse plane, cell nuclei are stained with DAPI (blue). Looking at the magnified region in the white box, both MACROH2A1 and MAP4 transcripts are detected outside of DAPI positive nuclei and in the white matter. **(B)** Sagittal section of spinal cord revealing axons are immunostained with β-III tubulin (Blue) and RNAscope detection of MACROH2A1 (Red), revealing the presence of this RNA transcript along the axons.

(Figure 6). In an effort to find additional putative circRNAs altered following SCI, we annotated our data and found over 200 circRNA that were significantly modulated after SCI (see Tables 5A,B). To better understand the potential role that circRNAs play in axonal growth, we modulated the level of ADAR1,that inhibits the formation of circRNA. Using siRNA to block ADAR1 expression we show that cortical neurons grow more abundant and longer axons (Figure 7). This finding directly suggests that up-regulating the formation of circRNA leads to longer axonal outgrowth and suggests reduction of these circRNAs following SCI impairs axon regeneration. We used RNAscope to confirm the expression of circRims2 RNA in spinal cord tissue. In combination with RbnR treatment that digests linear mRNA, such as GAP-43, but does not affect circRNA, we found that Rims2 expression was preserved in the tissue (Figure 8). While little is known about the role of circRNAs in neuronal function, both miRNA and RNA-binding protein (RBP) binding functions have been described for circRNA. In addition, there are several other noted functions, including being transcriptional regulators and binding to ribosomes directly.

To identify potential mechanisms underlying circRNA on axon growth, we used bioinformatic analyses to predict which miR and RBPs could be binding to circRims2. We found multiple likely miRNAs that could bind to circRims2 that have also been reported to either target known mRNAs that modulates axonal regeneration

TABLE 5 (A, B) – List of putative circRNA detected by our RNA-seq.

| DEG | No-SCI | SCI | *p*-Adj | Log2 Fold |
|---|---|---|---|---|
| A | Downregulated | | | |
| circRNA | | | | |
| GRM5 | 23.29577 | 2.694973 | **7.65E-07** | −3.111725 |
| GRM3 | 102.725 | 18.6941 | **4.31E-08** | −2.458133 |
| SYN1 | 30.3644 | 6.49934 | **0.0001** | −2.224016 |
| MAGI1 | 214.236 | 52.34484 | **0.0006** | −2.033082 |
| ZKSCAN1 | 30.0316 | 8.962 | **0.01046** | −1.744589 |
| ASPH | 104.0453 | 36.66751 | **1.07E-05** | −1.504637 |
| RIMS2 | 183.564 | 68.53002 | **0.00026** | −1.421475 |
| TRIM2 | 324.4108 | 130.2952 | **0.00255** | −1.316038 |
| NCAM2 | 7.72297 | 3.106897 | **0.00158** | −1.313681 |
| NCAM1 | 202.4714 | 82.64531 | **2.51E-06** | −1.292713 |
| RTN4 | 137.3176 | 53.3194 | **0.00477** | −1.364784 |
| B | Up-regulated | | | |
| circRNA | | | | |
| FOXO3 | 25.1336 | 59.5538 | **0.00924** | 1.244576 |
| TCF12 | 33.516 | 85.27979 | **0.00676** | 1.347501 |
| VAPA | 171.73 | 445.116 | **0.04151** | 1.374039 |
| PRRX1 | 24.0978 | 63.6758 | **0.00119** | 1.401844 |
| UCK2 | 18.7675 | 64.8097 | **1.43E-07** | 1.787973 |
| COL3A1 | 2.31731 | 11.5008 | **2.20E-06** | 2.311211 |
| FOXP1 | 25.43917 | 147.0716 | **0.00034924** | 2.531395 |
| GDA | 6.73558 | 51.191 | **1.07E-06** | 2.926016 |
| CLMP | 1.574086 | 15.92662 | **3.56E-11** | 3.338854 |

From our analysis, we have detected over 200 putative circRNA. We made a short list of the 20 with the most significant *p*-Adj values. The circRNA above the line are down-regulated after SCI are displayed in A and the ones that are up-regulated are displayed in B.

or has been shown to mediate SCI-injury (see Table 6). Circular RNA interactome predict the miRNAs that can bind to circRims2 (Dudekula et al., 2016). Of those predicted miRNAs two can also bind to the 3'UTR of GAP-43, an mRNA known to be transported into axons for local translation. They are miR-192 and -377, each having 8 or 7 predicted binding sites, respectively, to circRims2. Axonally translated GAP-43 supports axonal elongation (Willis et al., 2005) and we detect GAP-43 mRNA in the axons by RNAscope.

Yayon et al. utilize a method called Patch-Seq analysis which is single-cell RNA-seq from fixed tissues using iDISCO and advanced microscopy (NuNeX) to help spatially select VChIs neurons and detect changes in dendritic regions of these neurons after whisker deprivation model (Yayon et al., 2023). By doing so, they have detected dendrite localized transcripts such as Elmo1, Msi2 and Tubb3 (β-III tubulin) which are down-regulated, while Arpp21 and Sema5b are up-regulated. From our findings, we observed that Tubb3 and Sema5b, which are detected in both dendrites and axons, go down significantly after injury. We detect no significant changes in Elmo1 or Msi2. Intriguingly, Arpp21 goes down significantly after injury in our RNA-seq, by 4-fold and it is a putative circRNA. Further analyses are required to have a better understanding the consequences of these changes in potentially dendritic and axonal signatures. Similar to other reports such as Hanan et al. looking at circSLC8A1 in a Parkinson's Disease model, we will follow-up our findings of circRims2 to elucidate it's molecular mechanism to potentially modulate axonal outgrowth and to determine the miRNA and/or RBPs that it could be binding to for regulation of this outgrowth (Hanan et al., 2020).

These observations predict a RNA-based regulatory pathway from circRNA Rims2 → miRNA (miR-192 or −377) → GAP-43 mRNA to control axonal levels of GAP-43 protein and regulate axonal outgrowth (Figure 9). The decreased levels of circRims2 after SCI indicate that there may local internal RNA- mechanisms that control axonal regeneration and RNA based therapies could play a role in neurorepair.

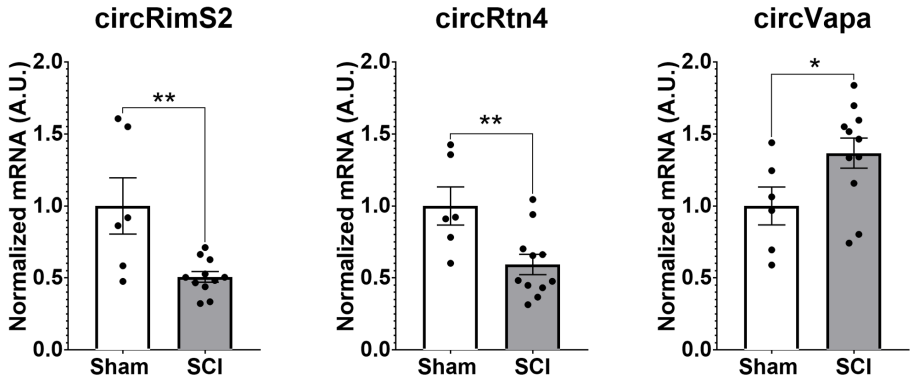


FIGURE 6
Validation by RT-qPCR in combination with RbnR treatment for identification of circRNA from mouse spinal cord. Using mouse spinal cord from animals with ($N$ =11) and without contusions ($N$ =6) at 14days post injury, we combined RbnR treatment and RT-qPCR for detection of circRims2, circRtn4 and circVAPA. We found that the trends were the same as in the RNA-seq dataset, in that both circRims2 and circRtn4 were down-regulated while circVAPA was up-regulated. CircRNA changes are significant as determined by $t$-test with $^{**}p$ <0.01 and $^{*}p$ <0.05.

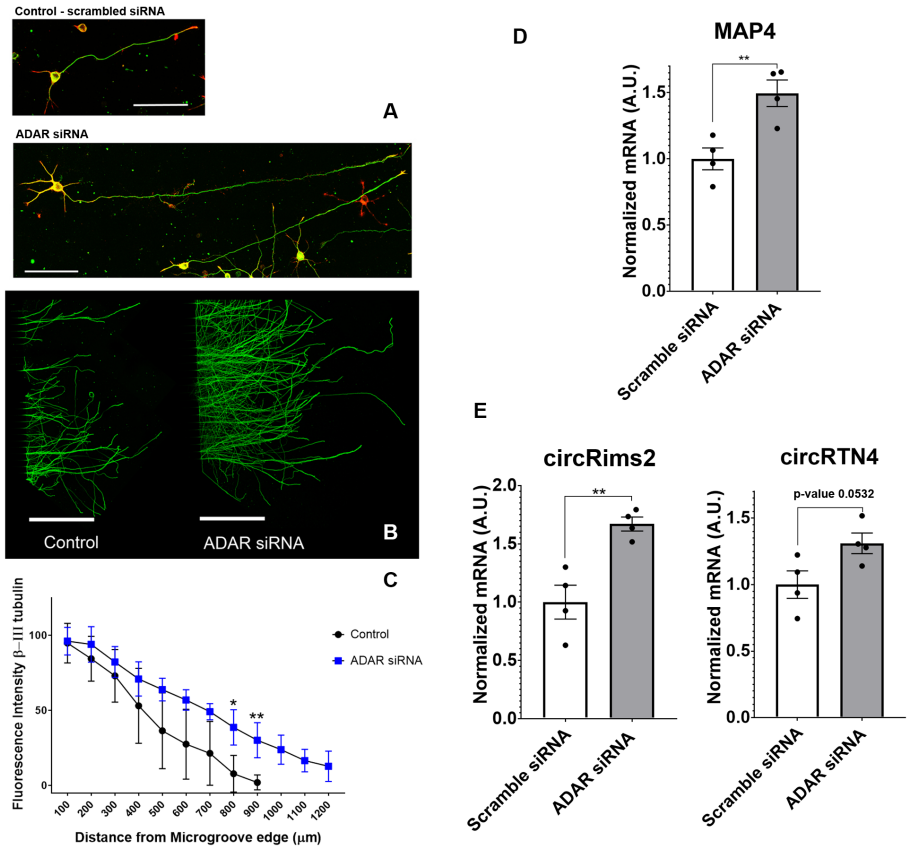


FIGURE 7
Treatment with siRNA against ADAR1 compared to scrambled controls promote longer axons in rat primary cortical neurons. **(A)** Axons were stained with β-III tubulin (green) antibodies and actin (red) stain. **(B)** Bottom panel, Cortical neurons in microfluidic chambers longer axons with ADAR 1 siRNA compared to scrambled controls, Scale right panels 20 μm and microfluidic chambers in left panel 500 μm. **(C)** The graph is the average of 4 independent experiments in the microfluidic chambers and data points are the average with standard deviation. Statistics is *t*-test (*$p < 0.05$ and **$p < 0.01$) comparing Control to ADAR siRNA (blue) at a fixed distance in the microgrooves. At 800 and 900 microns, ADAR siRNA (blue) were growing significantly longer compared to controls. The graph is also displayed in Supplementary Figure 2, where we show the distribution of points for each condition. **(D)** In 4 independent experiments we targeted ADAR with siRNA and observed by RT-qPCR that MAP4 goes up significantly compared to scrambled controls. **(E)** By RT-qPCR in combination with Ribonuclease R to specifically detect circRNA, we observed up-regulation of both circRims2 (very significant) and circRTN4 (nearly significant, *p*-value 0.0532).

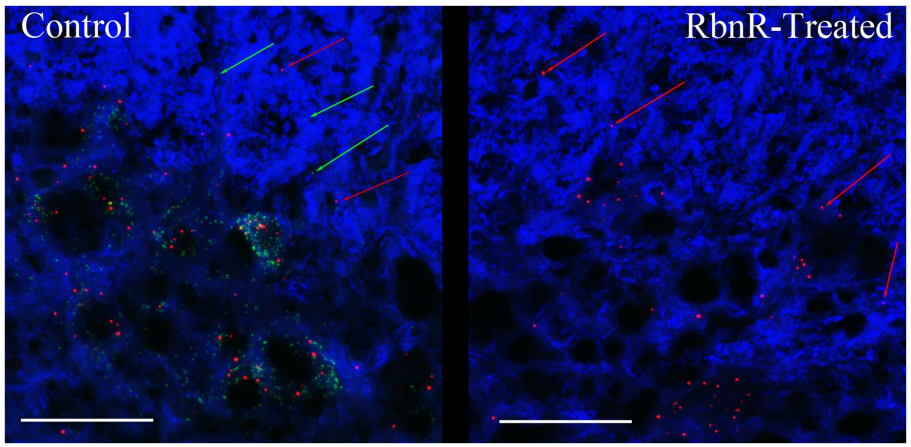


FIGURE 8
circRims2 is detected in rat spinal cord by RNAscope. Uninjured spinal cord section probed by RNAscope for GAP-43 (green) and Rims2 (red) transcripts and for with β-III tubulin (blue) immunohistochemistry. Adjacent sections were processed identically except that one was treated with RbnR to remove all linear transcripts, such as GAP-43 and preserve circRNAs. In the control (left) we detect both GAP-43 (green arrows) and Rims2 (red arrows). With RbnR-treatment, only the circRims2 remains and GAP-43 is undetected (right).

TABLE 6 Predicted miR that can bind to circRims2.

| miRNA predictions | #binding sites | Mediated effects | Targets |
|---|---|---|---|
| miR-495 | 31 | | STAT3 |
| miR-494 | 21 | | Nogo |
| miR-142-5p | 13 | Detected in sera of patients with SCI | |
| miR-145 | 12 | Negative regulator of astrogliosis | |
| miR-21 | 10 | Regulate Axon Growth | BDNF;PTEN |
| miR-431 | 10 | Enhances axonal regeneration | Wnt signalling |
| miR-155 | 8 | Deletion promotes longer neurites | CREB1 |
| miR-331-3p | 8 | Attenuates neuropathic pain | RAP1A |
| miR-192 | 8 | | GAP-43 |
| miR-377 | 7 | | GAP-43 |

Using Circular RNA Interactome, we predicted which miR can bind to circRims2 and the number of binding sites. We present miR that are known to mediate SCI injury or whose targets are a known protein that is an effector for axonal regeneration.

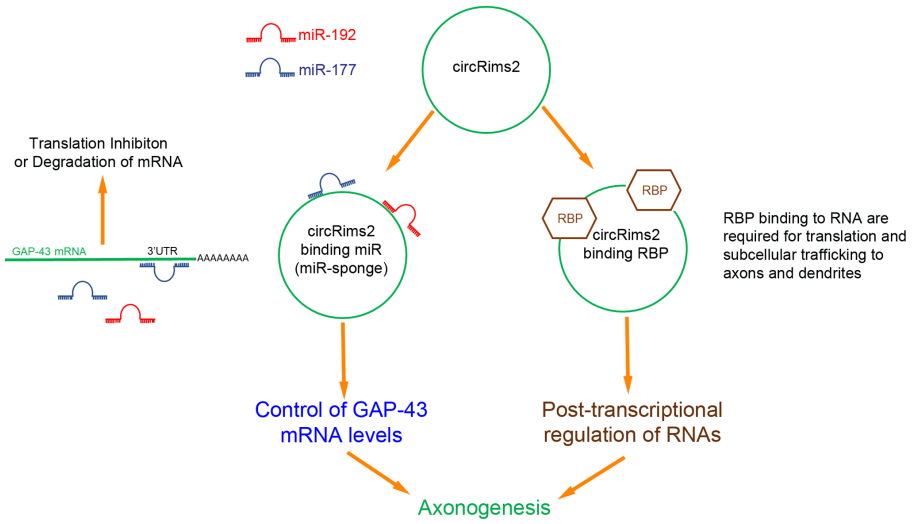


FIGURE 9
Inferred RNA pathway for circRims2 in modulating axonogenesis. By data mining, we identified 18 miR that could bind to circRims2 including miR-192 (red) and miR-177 (blue) that can target the 3'UTR of GAP-43 mRNA. mRNA bound to miR are either inhibited from being translated or degraded. circRNAs have been described to be miR-sponges. circRims2 could competitively bind miR-192 and -177 and prevent them from binding to GAP-43 mRNA, controlling expression of GAP-43 and promoting axonal outgrowth. circRims2 could also bind to RBPs, such as FUS that are known to mediate axonal outgrowth. RBPs can be involved in subcellular trafficking of RNA to axons and dendrites. RBPs are known to also regulate translation, hence another putative mechanism for regulating axonogenesis.

## Data availability statement

The datasets presented in this study can be found in online repositories. The names of the repository/repositories and accession number(s) can be found at: https://www.ncbi.nlm.nih.gov/, GSE230066.

## Ethics statement

The animal study was reviewed and approved by the IACUC at Icahn School of Medicine at Mount Sinai and James J. Peters VA Hospital.

## Author contributions

MS developed all conceptual ideas, analyzed and assisted with all experiments, microscopy, and wrote the manuscript. CT assisted with all *in vivo* experiments, RT-qPCR, and preparation of RNA for RNA-seq. NJ assisted with all *in vitro* experiments, RNA-scope, preparation of primary neuronal cultures, and blinded quantification of data. JH performed all RNA-seq data analysis. YX assisted with circular RNA Interactome analysis. WM assisted with all RNA analysis. RT assisted with all *in vitro* experiments, preparation of primary neuronal cultures and RNA-scope. KJ assisted with *in vivo* experiments and RT-qPCR. GJ assisted with RNA-scope. ZS performed all blinded analysis of

RNA-scope experiments. LH assisted with *in vivo* experiments. JD assisted with mouse primary neuronal cultures and RT-qPCR. KB performed RNA-seq experiments. RS performed RNA-seq experiments. DW assisted with RNA analysis and critical editing of the manuscript. CC assisted with developing the conceptual ideas for the experiments and critically reviewed the manuscript. RI developed the conceptual ideas for the experiments and critically reviewed the manuscript. All authors contributed to the article and approved the submitted version.

## Funding

This work was supported by NIH grant GM 137056 and NYS Spinal Cord Injury Research Program Contract number #C34460GG.

## Acknowledgments

The authors would like to thank Soheila Karimi at the University of Manitoba, Winnipeg, Canada for assistance with oligodendrocyte markers and Stella Tsirka at Stony Brook University, USA for assistance with microglial cell markers. We also thank Bindu Sundaresan, Connie Zhang and Jacqueline Giliberti at ACD for their assistance with RNA-scope detection of circRims2.

## Conflict of interest

The authors declare that the research was conducted in the absence of any commercial or financial relationships that could be construed as a potential conflict of interest.

## Publisher's note



## Supplementary material

The Supplementary material for this article can be found online at: https://www.frontiersin.org/articles/10.3389/fnmol.2023.1183315/full#supplementary-material

SUPPLEMENTARY FIGURE 1
Up- and down-regulated biological processes by GO analysis. From our RNA-seq we used GO analysis to determine biological processes that are being regulated. In the top figure in gold are pathways that are significantly up-regulated when comparing control to SCI. The lower figure in blue are pathways that are significantly downregulated. The red arrows are pointing to pathways known to be involved with neurons.

SUPPLEMENTARY FIGURE 2
siRNA against ADAR1 compared to scrambled controls promote longer axons in rat primary cortical neurons- Graph from Figure 6C is replotted to show the distribution of points. This graph is the average of four independent experiments with standard deviations. Statistics is *t*-test (**p* <0.05 and ***p* <0.01) comparing Control to ADAR siRNA (blue) at a fixed distance in the microgrooves. At 800 and 900 microns, DAR siRNA (blue) were significantly longer compared to controls.

SUPPLEMENTARY FIGURE 3
Detection of ribosomes in the axons and growth cone tips of rat cortical neurons. We confirm expression of ribosomes in our cortical neurons by immunohistochemistry using an antibody against S6 Ribosomal Protein (green). We use Actin-Red to visualize the growth cones (white arrow). Dapi (blue) is staining the cell bodies and β-III tubulin immunohistochemistry to see the axons is in white.

SUPPLEMENTARY FIGURE 4
Prediction of 7 RBPs binding to circRims2. Using Circular RNA Interactome we predicted 7 RBPs that could bind to circRims2. The number in each column represents the number of binding sites. Fused in Sarcoma (FUS) has 16 binding sites on circRims2. FUS has been suggested to be involved in neurite outgrowth and axonal transport (70–73).

## References

Adam, M., Potter, A. S., and Potter, S. S. (2017). Psychrophilic proteases dramatically reduce single-cell RNA-seq artifacts: a molecular atlas of kidney development. *Development* 144, 3625–3632. doi: 10.1242/dev.151142

Adams, K. L., Rousso, D. L., Umbach, J. A., and Novitch, B. G. (2015). Foxp1-mediated programming of limb-innervating motor neurons from mouse and human embryonic stem cells. *Nat. Commun.* 6:6778. doi: 10.1038/ncomms7778

Akum, B. F., Chen, M., Gunderson, S. I., Riefler, G. M., Scerri-Hansen, M. M., and Firestein, B. L. (2004). Cypin regulates dendrite patterning in hippocampal neurons by promoting microtubule assembly. *Nat. Neurosci.* 7, 145–152. doi: 10.1038/nn1179

Balabanian, L., Chaudhary, A. R., and Hendricks, A. G. (2018). Traffic control inside the cell: microtubule-based regulation of cargo transport. *Biochemist* 40, 14–17. doi: 10.1042/BIO04002014

Baleriola, J., Walker, C. A., Jean, Y. Y., Crary, J. F., Troy, C. M., Nagy, P. L., et al. (2014). Axonally synthesized ATF4 transmits a neurodegenerative signal across brain regions. *Cells* 158, 1159–1172. doi: 10.1016/j.cell.2014.07.001

Basso, D. M., Beattie, M. S., and Bresnahan, J. C. (1995). A sensitive and reliable locomotor rating scale for open field testing in rats. *J. Neurotrauma* 12, 1–21. doi: 10.1089/neu.1995.12.1

Birsa, N., Ule, A. M., Garone, M. G., Tsang, B., Mattedi, F., Chong, P. A., et al. (2021). FUS-ALS mutants alter FMRP phase separation equilibrium and impair protein translation. *Sci. Adv.* 7. doi: 10.1126/sciadv.abf8660

Bradl, M., and Lassmann, H. (2010). Oligodendrocytes: biology and pathology. *Acta Neuropathol.* 119, 37–53. doi: 10.1007/s00401-009-0601-5

Cao, Z., Harvey, S. S., Chiang, T., Foltz, A. G., Lee, A. G., Cheng, M. Y., et al. (2021). Unique subtype of microglia in degenerative thalamus after cortical stroke. *Stroke* 52, 687–698. doi: 10.1161/STROKEAHA.120.032402

Chen, E. Y., Tan, C. M., Kou, Y., Duan, Q., Wang, Z., Meirelles, G. V., et al. (2013). Enrichr: interactive and collaborative HTML5 gene list enrichment analysis tool. *BMC Bioinform.* 14:128. doi: 10.1186/1471-2105-14-128

Chiodi, V., Domenici, M. R., Biagini, T., De Simone, R., Tartaglione, A. M., Di Rosa, M., et al. (2021). Systemic depletion of histone macroH2A1.1 boosts hippocampal synaptic plasticity and social behavior in mice. *FASEB J.* 35:e21793. doi: 10.1096/fj.202100569R

Cosker, K. E., Fenstermacher, S. J., Pazyra-Murphy, M. F., Elliott, H. L., and Segal, R. A. (2016). The RNA-binding protein SFPQ orchestrates an RNA regulon to promote axon viability. *Nat. Neurosci.* 19, 690–696. doi: 10.1038/nn.4280

Curtis, R., Green, D., Lindsay, R. M., and Wilkin, G. P. (1993). Up-regulation of GAP-43 and growth of axons in rat spinal cord after compression injury. *J. Neurocytol.* 22, 51–64. doi: 10.1007/BF01183975

Dobin, A., Davis, C. A., Schlesinger, F., Drenkow, J., Zaleski, C., Jha, S., et al. (2013). STAR: ultrafast universal RNA-seq aligner. *Bioinformatics* 29, 15–21. doi: 10.1093/bioinformatics/bts635

Donnelly, C. J., Park, M., Spillane, M., Yoo, S., Pacheco, A., Gomes, C., et al. (2013). Axonally synthesized β-actin and GAP-43 proteins support distinct modes of axonal growth. *J. Neurosci.* 33, 3311–3322. doi: 10.1523/JNEUROSCI.1722-12.2013

Doster, S. K., Lozano, A. M., Aguayo, A. J., and Willard, M. B. (1991). Expression of the growth-associated protein GAP-43 in adult rat retinal ganglion cells following axon injury. *Neuron* 6, 635–647. doi: 10.1016/0896-6273(91)90066-9

Dudekula, D. B., Panda, A. C., Grammatikakis, I., De, S., Abdelmohsen, K., and Gorospe, M. (2016). CircInteractome: a web tool for exploring circular RNAs and their interacting proteins and microRNAs. *RNA Biol.* 13, 34–42. doi: 10.1080/15476286.2015.1128065

Dulin, J. N., Antunes-Martins, A., Chandran, V., Costigan, M., Lerch, J. K., Willis, D. E., et al. (2015). Transcriptomic approaches to neural repair. *J. Neurosci.* 35, 13860–13867. doi: 10.1523/JNEUROSCI.2599-15.2015

Escartin, C., Galea, E., Lakatos, A., O'Callaghan, J. P., Petzold, G. C., Serrano-Pozo, A., et al. (2021). Reactive astrocyte nomenclature, definitions, and future directions. *Nat. Neurosci.* 24, 312–325. doi: 10.1038/s41593-020-00783-4

Filbin, M. T. (2003). Myelin-associated inhibitors of axonal regeneration in the adult mammalian CNS. *Nat. Rev. Neurosci.* 4, 703–713. doi: 10.1038/nrn1195

Gaudet, A. D., Fonken, L. K., Watkins, L. R., Nelson, R. J., and Popovich, P. G. (2018). MicroRNAs: roles in regulating Neuroinflammation. *Neuroscientist* 24, 221–245. doi: 10.1177/1073858417721150

Gaudet, A. D., Mandrekar-Colucci, S., Hall, J. C., Sweet, D. R., Schmitt, P. J., Xu, X., et al. (2016). miR-155 deletion in mice overcomes neuron-intrinsic and neuron-extrinsic barriers to spinal cord repair. *J. Neurosci.* 36, 8516–8532. doi: 10.1523/JNEUROSCI.0735-16.2016

Gene Ontology Consortium (2021). The gene ontology resource: enriching a GOld mine. *Nucleic Acids Res.* 49, D325–D334. doi: 10.1093/nar/gkaa1113

Gong, H., Dong, W., Rostad, S. W., Marcovina, S. M., Albers, J. J., Brunzell, J. D., et al. (2013). Lipoprotein lipase (LPL) is associated with neurite pathology and its levels are markedly reduced in the dentate gyrus of Alzheimer's disease brains. *J. Histochem. Cytochem.* 61, 857–868. doi: 10.1369/0022155413505601

Gracias, N. G., Shirkey-Son, N. J., and Hengst, U. (2014). Local translation of TC10 is required for membrane expansion during axon outgrowth. *Nat. Commun.* 5:3506. doi: 10.1038/ncomms4506

Guo, W., Naujock, M., Fumagalli, L., Vandoorne, T., Baatsen, P., Boon, R., et al. (2017). HDAC6 inhibition reverses axonal transport defects in motor neurons derived from FUS-ALS patients. *Nat. Commun.* 8:861. doi: 10.1038/s41467-017-00911-y

Hanan, M., Simchovitz, A., Yayon, N., Vaknine, S., Cohen-Fultheim, R., Karmon, M., et al. (2020). A Parkinson's disease CircRNAs resource reveals a link between circSLC8A1 and oxidative stress. *EMBO Mol. Med.* 12:e11942. doi: 10.15252/emmm.201911942

Hansen, J., Galatioto, J., Caescu, C. I., Arnaud, P., Calizo, R. C., Spronck, B., et al. (2019). Systems pharmacology-based integration of human and mouse data for drug repurposing to treat thoracic aneurysms. *JCI Insight*. 4:e127652. doi: 10.1172/jci.insight.127652

Hegarty, S. V., Wyatt, S. L., Howard, L., Stappers, E., Huylebroeck, D., Sullivan, A. M., et al. (2017). Zeb2 is a negative regulator of midbrain dopaminergic axon growth and target innervation. *Sci. Rep.* 7:8568. doi: 10.1038/s41598-017-08900-3

Ishigaki, S., and Sobue, G. (2018). Importance of functional loss of FUS in FTLD/ALS. *Front. Mol. Biosci.* 5:44. doi: 10.3389/fmolb.2018.00044

Ivanov, A., Memczak, S., Wyler, E., Torti, F., Porath, H. T., Orejuela, M. R., et al. (2015). Analysis of intron sequences reveals hallmarks of circular RNA biogenesis in animals. *Cell Rep.* 10, 170–177. doi: 10.1016/j.celrep.2014.12.019

Kaeser, P. S., Deng, L., Fan, M., and Südhof, T. C. (2012). RIM genes differentially contribute to organizing presynaptic release sites. *Proc. Natl. Acad. Sci. U. S. A.* 109, 11830–11835. doi: 10.1073/pnas.1209318109

Kang, R. B., Li, Y, Rosselot, C., Zhang, T., Siddiq, M., Rajbhandari, P., et al. (2023). Single nucleus RNA sequencing of human pancreatic islets identifies novel gene sets and distinguishes β-cell subpopulations with dynamic transcriptome profiles. *Genome Med.* 15, 1–24. doi: 10.1186/s13073-023-01179-2

Kar, A. N., Lee, S. J., Sahoo, P. K., Thames, E., Yoo, S., Houle, J. D., et al. (2021). MicroRNAs 21 and 199a-3p regulate axon growth potential through modulation of *Pten* and *mTor* mRNAs. *eNeuro.* 8. doi: 10.1523/ENEURO.0155-21.2021

Kar, A. N., Lee, S. J., and Twiss, J. L. (2018). Expanding axonal transcriptome brings new functions for Axonally synthesized proteins in health and disease. *Neuroscientist* 24, 111–129. doi: 10.1177/1073858417712668

König, N., Åkesson, E., Telorack, M., Vasylovska, S., Ngamjariyawat, A., Sundström, E., et al. (2011). Forced Runx1 expression in human neural stem/progenitor cells transplanted to the rat dorsal root ganglion cavity results in extensive axonal growth specifically from spinal cord-derived neurospheres. *Stem Cells Dev.* 20, 1847–1857. doi: 10.1089/scd.2010.0555

Kristensen, L. S., Andersen, M. S., Stagsted, L. V. W., Ebbesen, K. K., Hansen, T. B., and Kjems, J. (2019). The biogenesis, biology and characterization of circular RNAs. *Nat. Rev. Genet.* 20, 675–691. doi: 10.1038/s41576-019-0158-7

Li, Y., Ma, W. G., and Li, X. C. (2021). Identification of blood miR-216a, miR-377 and their target genes ANGPTL4, GAP-43 and serum of PPARG as biomarkers for diabetic peripheral neuropathy of type 2 diabetes. *Clin. Lab.* 67. doi: 10.7754/Clin.Lab.2020.191220

Liu, X., Cui, X., Guan, G., Dong, Y., and Zhang, Z. (2020). microRNA-192-5p is involved in nerve repair in rats with peripheral nerve injury by regulating XIAP. *Cell Cycle* 19, 326–338. doi: 10.1080/15384101.2019.1710916

Memczak, S., Jens, M., Elefsinioti, A., Torti, F., Krueger, J., Rybak, A., et al. (2013). Circular RNAs are a large class of animal RNAs with regulatory potency. *Nature* 495, 333–338. doi: 10.1038/nature11928

Miron, V. E., Kuhlmann, T., and Antel, J. P. (2011). Cells of the oligodendroglial lineage, myelination, and remyelination. *Biochim. Biophys. Acta* 1812, 184–193. doi: 10.1016/j.bbadis.2010.09.010

Mocchetti, I., and Wrathall, J. R. (1995). Neurotrophic factors in central nervous system trauma. *J. Neurotrauma* 12, 853–870. doi: 10.1089/neu.1995.12.853

Nagelhus, E. A., and Ottersen, O. P. (2013). Physiological roles of aquaporin-4 in brain. *Physiol. Rev.* 93, 1543–1562. doi: 10.1152/physrev.00011.2013

Orozco, D., Tahirovic, S., Rentzsch, K., Schwenk, B. M., Haass, C., and Edbauer, D. (2012). Loss of fused in sarcoma (FUS) promotes pathological tau splicing. *EMBO Rep.* 13, 759–764. doi: 10.1038/embor.2012.90

Pico, A. R., Kelder, T., van Iersel, M. P., Hanspers, K., Conklin, B. R., and Evelo, C. (2008). WikiPathways: pathway editing for the people. *PLoS Biol.* 6:e184. doi: 10.1371/journal.pbio.0060184

Piwecka, M., Glažar, P., Hernandez-Miranda, L. R., Memczak, S., Wolf, S. A., Rybak-Wolf, A., et al. (2017). Loss of a mammalian circular RNA locus causes miRNA deregulation and affects brain function. *Science* 357. doi: 10.1126/science.aam8526

Raineteau, O., and Schwab, M. E. (2001). Plasticity of motor systems after incomplete spinal cord injury. *Nat. Rev. Neurosci.* 2, 263–273. doi: 10.1038/35067570

Raj, D., Yin, Z., Breur, M., Doorduin, J., Holtman, I. R., Olah, M., et al. (2017). Increased white matter inflammation in aging- and Alzheimer's disease brain. *Front. Mol. Neurosci.* 10:206. doi: 10.3389/fnmol.2017.00206

Riccio, A. (2018). RNA targeting and translation in axons. *Science* 359, 1331–1332. doi: 10.1126/science.aat1498

Rybak-Wolf, A., Stottmeister, C., Glažar, P., Jens, M., Pino, N., Giusti, S., et al. (2015). Circular RNAs in the mammalian brain are highly abundant, conserved, and dynamically expressed. *Mol. Cell* 58, 870–885. doi: 10.1016/j.molcel.2015.03.027

Schwabenland, M, Brück, W, Priller, J, Stadelmann, C, Lassmann, H, and Prinz, M. Analyzing microglial phenotypes across neuropathologies: a practical guide. *Acta Neuropathol.* (2021). 142:923–936. doi:10.1007/s00401-021-02370-8.; PMCID: PMC8498770.

Siddiq, M. M., Hannila, S. S., Carmel, J. B., Bryson, J. B., Hou, J., Nikulina, E., et al. (2015). Metallothionein-I/II promotes axonal regeneration in the central nervous system. *J. Biol. Chem.* 290, 16343–16356. doi: 10.1074/jbc.M114.630574

Siddiq, M. M., Hannila, S. S., Zorina, Y., Nikulina, E., Rabinovich, V., Hou, J., et al. (2021). Extracellular histones, a new class of inhibitory molecules of CNS axonal regeneration. *Brain Commun.* 3. doi: 10.1093/braincomms/fcab271

Sleigh, J. N., Rossor, A. M., Fellows, A. D., Tosolini, A. P., and Schiavo, G. (2019). Axonal transport and neurological disease. *Nat. Rev. Neurol.* 15, 691–703. doi: 10.1038/s41582-019-0257-2

Spaulding, E. L., and Burgess, R. W. (2017). Accumulating evidence for axonal translation in neuronal homeostasis. *Front. Neurosci.* 11:312. doi: 10.3389/fnins.2017.00312

Stillitano, F, Hansen, J, Kong, CW, Karakikes, I, Funck-Brentano, C, Geng, L, et al. (2017). Modeling susceptibility to drug-induced long QT with a panel of subject-specific induced pluripotent stem cells. *elife* 2017;6. pii::e19406. doi:10.7554/eLife.19406, 6.

Sugiyama, Y., Oishi, T., Yamashita, A., Murata, Y., Yamamoto, T., Takashima, I., et al. (2019). Neuronal and microglial localization of secreted phosphoprotein 1 (osteopontin) in intact and damaged motor cortex of macaques. *Brain Res.* 1714, 52–64. doi: 10.1016/j.brainres.2019.02.021

Sun, J., Song, Y., Chen, Z., Qiu, J., Zhu, S., Wu, L., et al. (2022). Heterogeneity and molecular markers for CNS glial cells revealed by single-cell transcriptomics. *Cell. Mol. Neurobiol.* 42, 2629–2642. doi: 10.1007/s10571-021-01159-3

Terenzio, M., Koley, S., Samra, N., Rishal, I., Zhao, Q., Sahoo, P. K., et al. (2018). Locally translated mTOR controls axonal local translation in nerve injury. *Science* 359, 1416–1421. doi: 10.1126/science.aan1053

Toro, C. A., Hansen, J., Siddiq, M. M., Johnson, K., Zhao, W., Azulai, D., et al. (2021). The human ApoE4 variant reduces functional recovery and neuronal sprouting after incomplete spinal cord injury in male mice. *Front. Cell. Neurosci.* 15:626192. doi: 10.3389/fncel.2021.626192

Trapnell, C., Williams, B. A., Pertea, G., Mortazavi, A., Kwan, G., van Baren, M. J., et al. (2010). Transcript assembly and quantification by RNA-seq reveals unannotated transcripts and isoform switching during cell differentiation. *Nat. Biotechnol.* 28, 511–515. doi: 10.1038/nbt.1621

van Hasselt, J. G. C., Rahman, R., Hansen, J., Stern, A., Shim, J. V., Xiong, Y., et al. (2020). Transcriptomic profiling of human cardiac cells predicts protein kinase inhibitor-associated cardiotoxicity. *Nat. Commun.* 11:4809. doi: 10.1038/s41467-020-18396-7

Vernes, S. C., Oliver, P. L., Spiteri, E., Lockstone, H. E., Puliyadi, R., Taylor, J. M., et al. (2011). Foxp2 regulates gene networks implicated in neurite outgrowth in the developing brain. *PLoS Genet.* 7:e1002145. doi: 10.1371/journal.pgen.1002145

Villarin, J. M., McCurdy, E. P., Martínez, J. C., and Hengst, U. (2016). Local synthesis of dynein cofactors matches retrograde transport to acutely changing demands. *Nat. Commun.* 7:13865. doi: 10.1038/ncomms13865

Vromman, M., Anckaert, J., Vandesompele, J., and Volders, P. J. (2022). CIRCprimerXL: convenient and high-throughput PCR primer Design for Circular RNA quantification. *Front. Bioinform.* 2:834655. doi: 10.3389/fbinf.2022.834655

Vromman, M., Yigit, N., Verniers, K., Lefever, S., Vandesompele, J., and Volders, P. J. (2021). Validation of circular RNAs using RT-qPCR after effective removal of linear RNAs by ribonuclease R. *Curr. Protoc.* 1:e181. doi: 10.1002/cpz1.181

Waller, T., Lee, S. J., and Sattlegger, E. (2012). Evidence that Yih1 resides in a complex with ribosomes. *FEBS J.* 279, 1761–1776. doi: 10.1111/j.1742-4658.2012.08553.x

Wang, S., Mustafa, M., Yuede, C. M., Salazar, S. V., Kong, P., Long, H., et al. (2020). Anti-human TREM2 induces microglia proliferation and reduces pathology in an Alzheimer's disease model. *J. Exp. Med.* 217:e20200785. doi: 10.1084/jem.20200785

Wang, Y., Sugita, S., and Sudhof, T. C. (2000). The RIM/NIM family of neuronal C2 domain proteins. Interactions with Rab3 and a new class of Src homology 3 domain proteins. *J. Biol. Chem.* 275, 20033–20044. doi: 10.1074/jbc.M909008199

Willis, D., Li, K. W., Zheng, J. Q., Chang, J. H., Smit, A. B., Kelly, T., et al. (2005). Differential transport and local translation of cytoskeletal, injury-response, and neurodegeneration protein mRNAs in axons. *J. Neurosci.* 25, 778–791. doi: 10.1523/JNEUROSCI.4235-04.2005

Willis, D. E., Xu, M., Donnelly, C. J., Tep, C., Kendall, M., Erenstheyn, M., et al. (2011). Axonal localization of transgene mRNA in mature PNS and CNS neurons. *J. Neurosci.* 31, 14481–14487. doi: 10.1523/JNEUROSCI.2950-11.2011

Wu, W., Ji, P., and Zhao, F. (2020). CircAtlas: an integrated resource of one million highly accurate circular RNAs from 1070 vertebrate transcriptomes. *Genome Biol.* 21:101. doi: 10.1186/s13059-020-02018-y

Yayon, N., Amsalem, O., Zorbaz, T., Yakov, O., Dubnov, S., Winek, K., et al. (2023). High-throughput morphometric and transcriptomic profiling uncovers composition of naïve and sensory-deprived cortical cholinergic VIP/CHAT neurons. *EMBO J.* 42:e110565. doi: 10.15252/embj.2021110565

Zeman, R. J., Bauman, W. A., Wen, X., Ouyang, N., Etlinger, J. D., and Cardozo, C. P. (2009). Improved functional recovery with oxandrolone after spinal cord injury in rats. *Neuroreport* 20, 864–868. doi: 10.1097/WNR.0b013e32832c5cc2